

How Active EMI Filter ICs Reduce Common-Mode Emissions in Single- And Three-Phase Applications (Part 2): Modeling Ferrite Chokes

by Timothy Hegarty, Texas Instruments, Phoenix, Ariz.

Complying with the electromagnetic compatibility (EMC) regulations intended to limit the levels of conducted emissions requires the insertion of an electromagnetic interference (EMI) filter between a switching regulator and its input source. Now, increasingly, a compact and efficient design of the EMI filter is one of the main challenges in a high-density switching regulator.

Multistage passive filters provide high rolloff and are widely used in high-power ac line applications where common-mode (CM) noise is usually more difficult to manage than differential-mode (DM) noise. The high CM noise signature at the switching frequency and its low-order harmonics originate from the large switch-node voltage swing and the high parasitic coupling capacitance from the switching devices to the grounded chassis structure. With the total Y-capacitance of the filter often limited by fault-safety requirements related to touch current or stored energy, the required CM choke inductance is necessarily quite high, thus impacting the size, weight and cost metrics of the overall filter design.

Part 1 of this article series^[1] included an overview of active EMI filter (AEF) techniques to diminish the reliance on bulky passive filter components. An AEF circuit can significantly reduce magnetic component and overall filter size vis-à-vis an equivalent passive filter, enabling higher-density filter designs for size-constrained applications. However, accurate characterization and modeling of the choke impedance is an essential step and of paramount importance in EMI filter design, as the choke impedance directly impacts filter attenuation performance (as well as loop stability in active designs).

Following a review of the impedance behavior of ferrite-cored magnetic components, this article describes a SPICE-compatible behavioral model for a ferrite choke using an intuitive circuit structure. This model facilitates easy and accurate system-level EMI simulations in the time and frequency domains for both passive and active filter designs.

Using an extraction procedure of model parameters based on small-signal impedance measurements, the synthesized behavioral model for the choke impedance can accommodate single-phase two-winding (1p2w), three-phase three-winding (3p3w) and three-phase four-winding (3p4w) chokes. The article concludes with a practical example to illustrate the modeling procedure applied to a 1p2w ferrite CM choke to simultaneously provide both high CM and high DM impedance in an EMI filter for a server rack power supply rated at 1 kW.

Review Of Passive And Active Filter Schematics

Intended as a foundational review from part 1, the schematics of Fig. 1 provide the framework for passive and active filter designs in kilowatt-scale, grid-connected applications, both single phase and three phase.

Fundamental to the active circuits in Fig. 1a and 1b are the TPSF12C1^[2] and TPSF12C3^[3] standalone AEF integrated circuits (ICs) from Texas Instruments, which operate in single-phase and three-phase systems, respectively.^[4]

As evident from Fig. 1, the active circuits can be derived from their passive filter counterparts by positioning the AEF IC and Y-rated injection capacitor at the filter center node (between the two CM chokes) to provide a low-impedance shunt path to ground for CM current. This then enables lower CM choke inductances for a given filter attenuation specification.

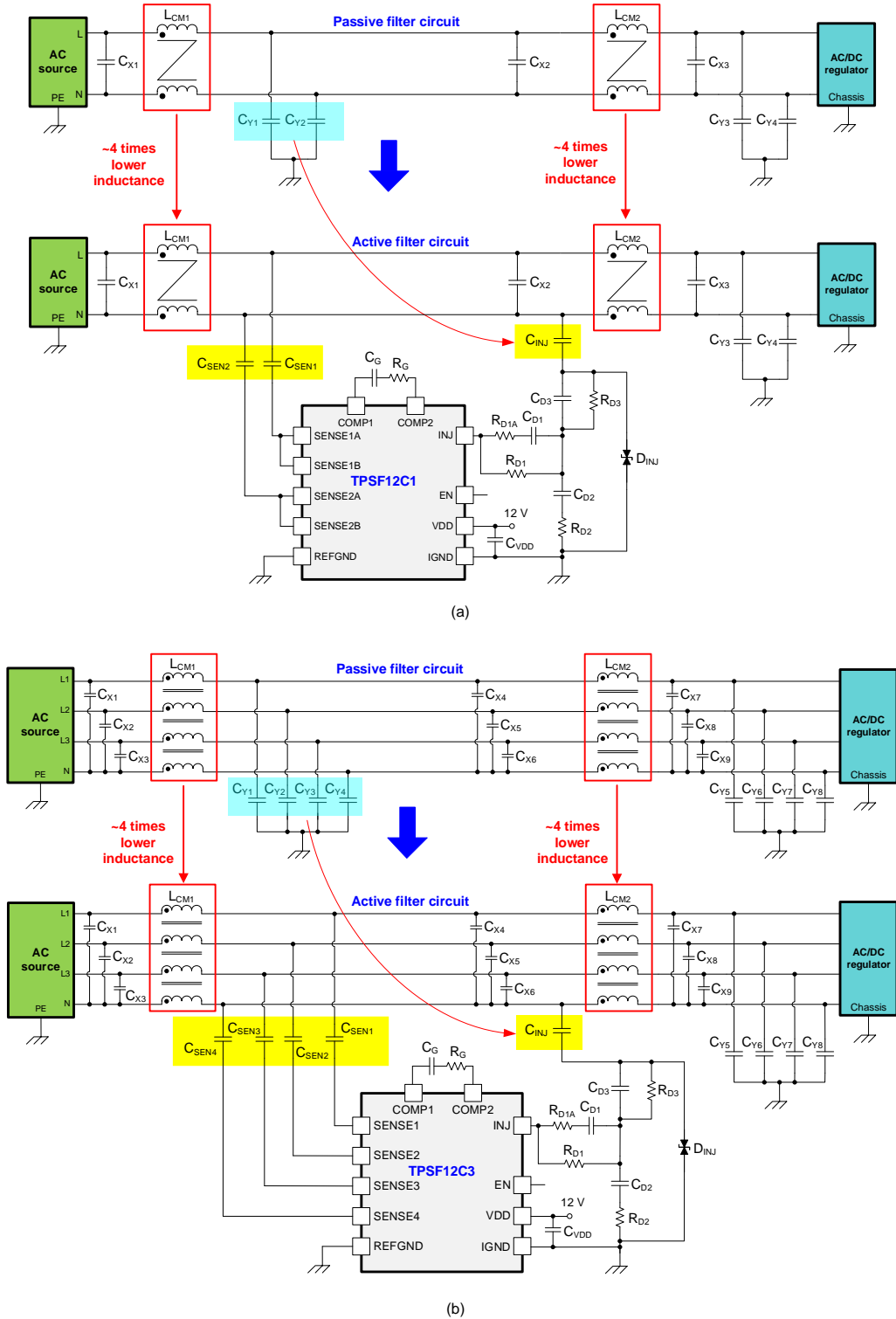


Fig. 1. Passive and active filter schematics for DM and CM noise attenuation: a 1p2w system (a) and a 3p4w system (b). Terminals L, N and PE refer to live, neutral and protective earth connections, respectively.

Central to the loop stability, attenuation performance and overall operation of active filter circuits is the impedance characteristic of the CM choke. With that in mind I'll now examine comprehensive simulation models for chokes with ferrite core material, with the objective of using these magnetic components in active filter circuits and realizing a substantial increase in efficiency and power density of the overall EMI filter.

By accurately reproducing the impedance frequency response, the simulation models can cater to a sufficiently broad frequency range for conducted emissions, exceeding 30 MHz or 108 MHz for commercial and automotive EMI standards, respectively.

Magnetic Components And Basic Equivalent Circuit Models

Fig. 2 shows basic lumped-element models for single-winding (two-terminal), two-winding (four-terminal) and three-winding (six-terminal) magnetic components: an inductor, a coupled DM inductor, and coupled CM inductors (more widely known, of course, as CM chokes). Here, L is the self-inductance of a single winding, M is the mutual inductance between a pair of windings, and k is the winding coupling factor.

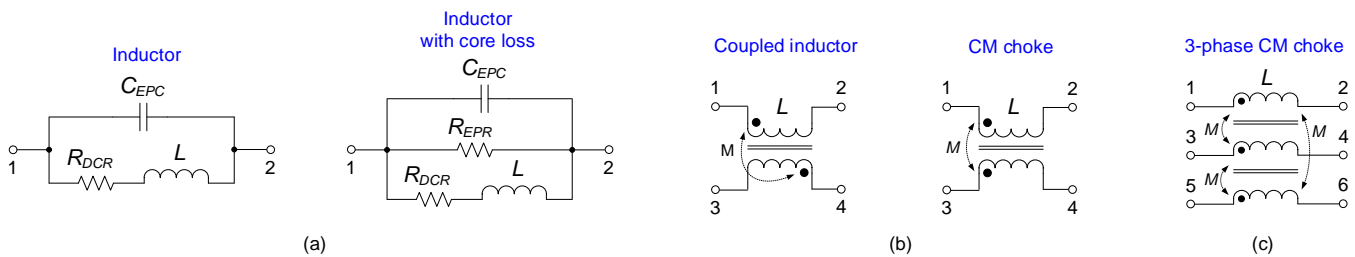


Fig. 2. Basic models for two-terminal (a), four-terminal (b) and six-terminal (c) magnetic components.

The upper sign in the expressions for L_{CM} and L_{DM} in equation 1 is for a CM choke, while the lower sign applies to a coupled DM inductor.^[5-7] For example, if $k = 0.98$ for a CM choke, then $L_{CM} = 0.99L$ and $L_{DM} = 0.04L$, where L_{CM} and L_{DM} are the CM and DM inductance contributions, respectively.

$$k = \frac{M}{\sqrt{L_1 L_2}} = \frac{M}{L}, \quad 0 \leq |k| \leq 1$$

$$L_{CM(2-winding)} = \frac{L \pm M}{2} = \frac{L(1 \pm k)}{2} \quad (1)$$

$$L_{DM(2-winding)} = 2(L \mp M) = 2L(1 \mp k)$$

The equivalent parallel resistance and capacitance, denoted as R_{EPR} and C_{EPC} in Fig. 2a, model the core loss and intrawinding parasitic capacitance, and determine the peak impedance value (or Q factor) and resonant frequency of the impedance characteristic, respectively.

Meanwhile, a three-phase power system may use a three- or four-winding CM choke,^[8,9] depending on the availability of a neutral connection. Fig. 3 highlights the DM and CM magnetic flux paths and current directions for a three-winding symmetrically wound CM choke using a toroidal core shape.^[8]

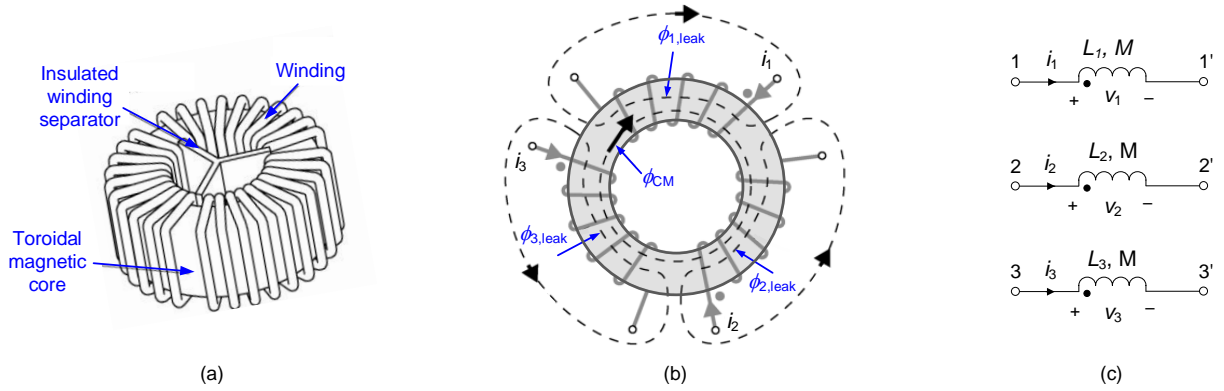


Fig. 3. A three-phase CM choke (a), relevant currents and magnetic fields (b), and schematic representation (c).

If $L_1 = L_2 = L_3 = L$, then equations 2 and 3 correspond to the inductance matrices:

$$\begin{bmatrix} v_{1,CM} \\ v_{2,CM} \\ v_{3,CM} \end{bmatrix} = \begin{bmatrix} L & M & M \\ M & L & M \\ M & M & L \end{bmatrix} \cdot \frac{d}{dt} \begin{bmatrix} i_{1,CM} \\ i_{2,CM} \\ i_{3,CM} \end{bmatrix} \quad (2)$$

$$\begin{bmatrix} v_{1,DM} \\ v_{2,DM} \\ v_{3,DM} \end{bmatrix} = \begin{bmatrix} L - M & 0 & 0 \\ 0 & L - M & 0 \\ 0 & 0 & L - M \end{bmatrix} \cdot \frac{d}{dt} \begin{bmatrix} i_{1,DM} \\ i_{2,DM} \\ i_{3,DM} \end{bmatrix} \quad (3)$$

Equation 4 describes the CM and DM inductances. The CM inductance relates to the three symmetrical currents $i_{1,CM} = i_{2,CM} = i_{3,CM} = i_{CM}$ giving $v_{1,CM} = v_{2,CM} = v_{3,CM} = v_{CM}$. Also, consider the three DM (or asymmetrical) currents $i_{1,DM} + i_{2,DM} + i_{3,DM} = 0$, giving $v_{1,DM} + v_{2,DM} + v_{3,DM} = 0$.

$$L_{CM(3-winding)} = \frac{v_{CM}}{di_{CM}/dt} = \frac{L + 2M}{3} = L \frac{1 + 2k}{3} \quad (4)$$

$$L_{DM(3-winding)} = \frac{v_{i,DM}}{di_{i,DM}/dt} = L - M = L(1 - k), \quad i = 1, 2, 3$$

Impedance Behavior Of Ferrite Chokes

Invented by J.L. Snoek in the 1940s at Phillips Research Labs in Eindhoven, Netherlands, and manufactured using low-cost ceramic processing techniques, soft ferrites are now indispensable in numerous power electronics applications.^[10,11] The near-insulating character of ferrites results in a nearly constant value of permeability over many decades of frequency, typically up to several megahertz for manganese-zinc (Mn-Zn) ferrites and above 10 MHz for nickel-zinc (Ni-Zn) ferrites. Other advantages include low core losses at high frequencies and cost-effective availability in a wide range of geometric shapes and sizes.

Fig. 4 shows the measured impedance magnitude and phase profiles versus frequency for an exemplary ferrite CM choke.

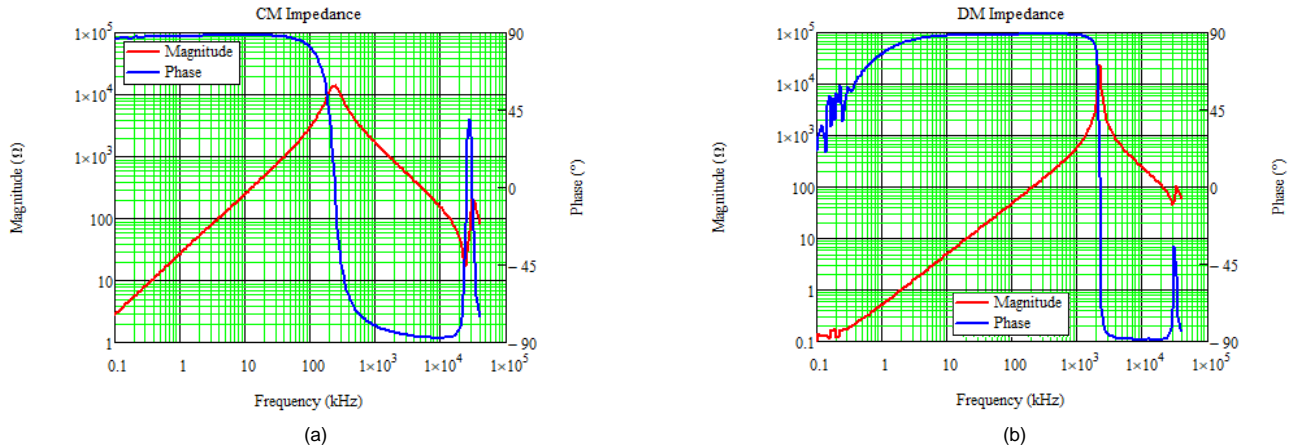


Fig. 4. Measured CM (a) and DM (b) impedance magnitude and phase characteristics of a ferrite-cored CM choke.

One or more higher-order resonances may appear in the measured choke impedances, arising from inner resonant behavior (for example, the inductance with the winding-turns-to-core capacitance). For added context, this particular example showcases a CM choke where the DM inductance is purposely increased using a ferrite sleeve above the normal 1% to 3% of L_{CM} typically obtained through the leakage inductance.^[12] Higher-order resonances notwithstanding, the asymptotes of the impedance magnitude characteristics in Fig. 4 appear at |20 dB| per decade at either side of the main self-resonant peak, and the phase characteristics display a high-Q transition from 90° to -90° at resonance.

The remainder of this article focuses on the derivation of an impedance behavioral model for ferrite chokes. Subsequently, part 3 in this article series will provide a detailed treatment for chokes with nanocrystalline core material, which require a different model structure from that of ferrite given the nonlinear characteristic of magnetic permeability with frequency.

Behavioral Model Structure For A Single-Phase Ferrite Choke

Because construction data and other basic parameters, such as properties of the core material, are seldom available from magnetic vendors or respective data sheets to create a physical model, let's instead focus on a behavioral model based on measured small-signal impedance (magnitude and phase) data for a choke.

Fig. 5 shows a simple behavioral circuit model of a two-winding, four-terminal choke.^[13] The CM and DM blocks separately represent the CM and DM impedances and use coupled inductors with positive coupling ($k_c = 1$) and negative coupling ($k_D = -1$), respectively. The choice of coupling coefficients is deliberately to avoid cross-coupling between the CM and DM blocks, such that the CM block presents zero impedance to DM current and vice versa. Assume that the windings have the same electrical parameters and are perfectly symmetric.

As expected, resistors designated as R_0 in the model represent the copper losses caused by dc and ac currents. R_C and R_D designate the core-loss resistances in CM and DM circuits, respectively, and represent the energy losses caused by hysteresis and eddy currents. Correspondingly, C_C and C_D represent the distributed parasitic self-capacitance of the windings for CM and DM emissions, respectively. Capacitors designated as C_W in the model denote the parasitic interwinding capacitance for improved high-frequency accuracy of the DM response.

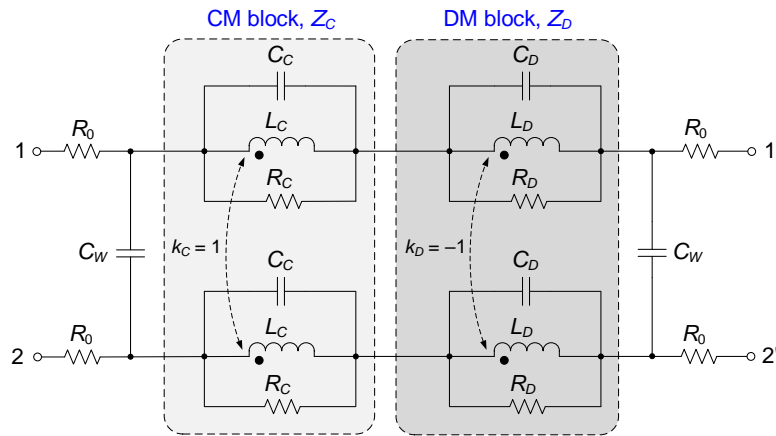


Fig. 5. Behavioral circuit model of a 1p2w ferrite choke with separate CM and DM blocks.

Fig. 6 illustrates the CM and DM circuit reductions from coupled inductor to separate uncoupled inductors and finally to a parallel RLC circuit arrangement, each equivalently expressing the CM and DM behaviors and current directions. As such, it is quite straightforward to transition from a four-terminal model (for a filter schematic) to a two-terminal model (for a CM or DM filter equivalent circuit).

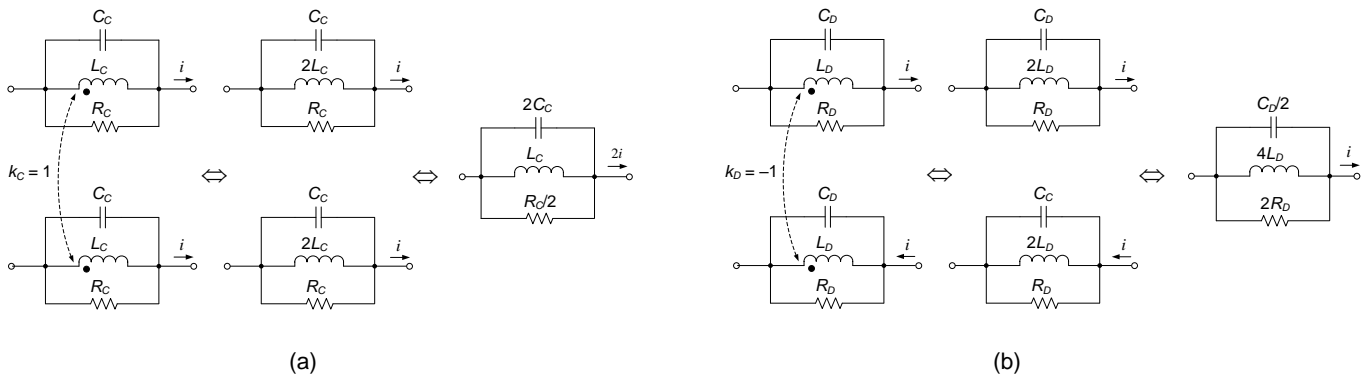


Fig. 6. Illustration of circuit reduction regarding the CM block for CM current (a) and the DM block for DM current (b).

More generally, Fig. 7 presents a comprehensive circuit model for a two-winding choke. Each block now contains one or more parallel RLC circuits connected in series to model the main and inner resonances.

For instance, inclusion of a second parallel RLC stage models the first anti-resonance and second resonance (as an example, see the 20-MHz to 30-MHz range in the impedance plots of Fig. 4). Embedding additional parallel RLC stages in series models higher-order resonances if needed.

By using the structure in Fig. 7, the modeled impedance of the choke fits precisely to the measured data across the full frequency range. In contrast, the traditional single parallel RLC equivalent model shown in Fig. 2a and Fig. 5 with core loss resistance and intrawinding capacitance models just one resonant peak. The DM impedance behavior characterizes in a similar fashion.

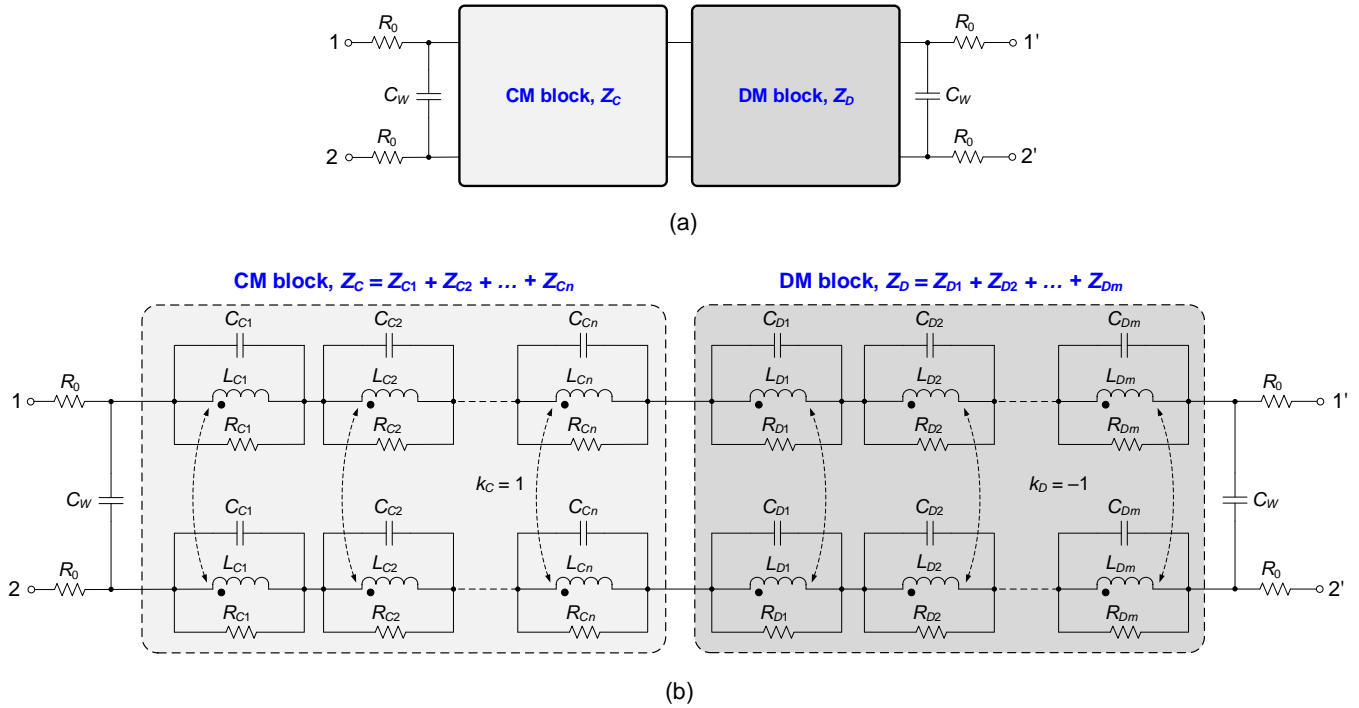
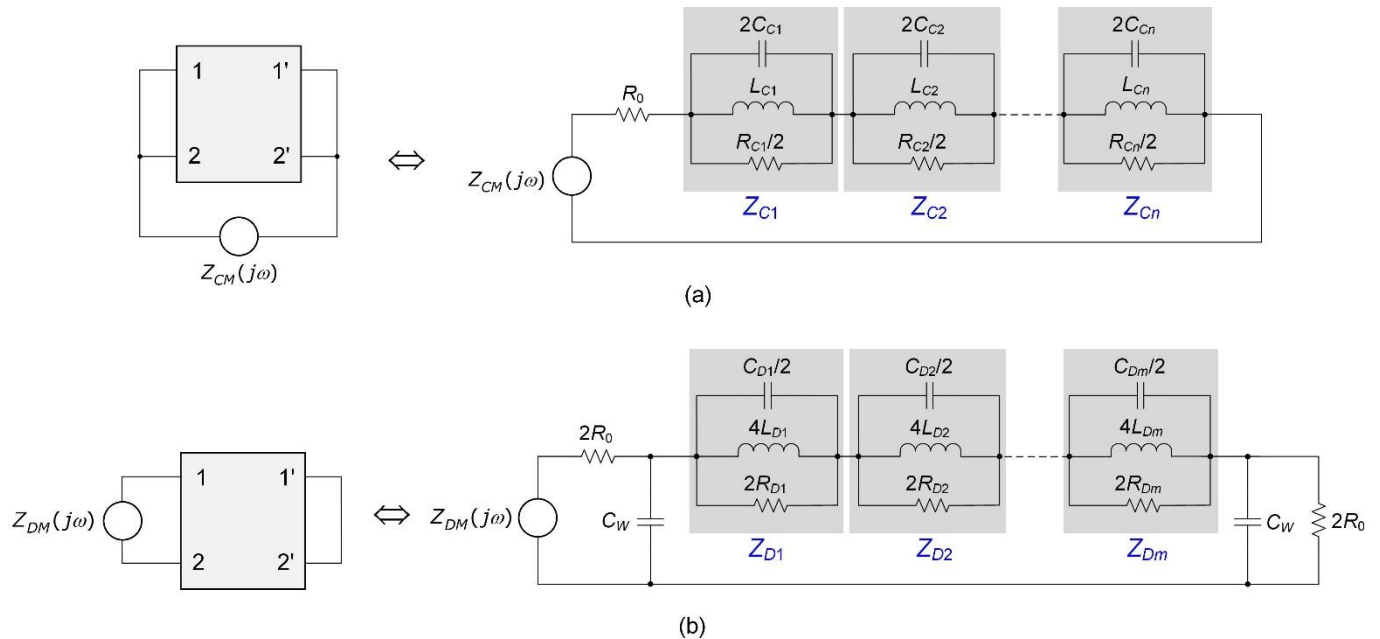


Fig. 7. Generalized choke model consisting of CM and DM blocks (a) with additional RLC elements to model high-frequency resonant behaviors (b).

Parameter Extraction For A Single-Phase Ferrite Choke

Fig. 8 illustrates measurement setups for CM, DM and open-circuit (OC) impedance tests to characterize a 1p2w choke. Also shown is the corresponding equivalent circuit for each test setup based on simplification of the model shown in Fig. 7b using the circuit reduction techniques from Fig. 6.



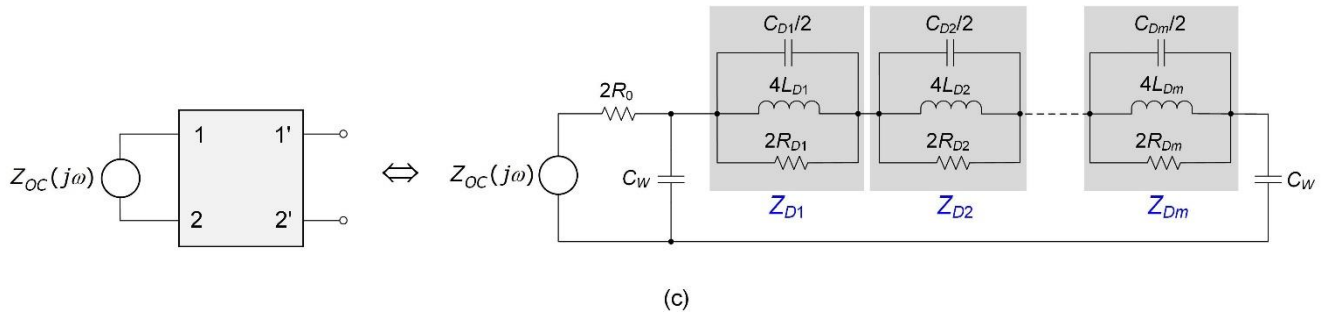


Fig. 8. Equivalent circuits corresponding to CM (a), DM (b) and OC (c) impedance measurement setups for model parameter extraction of a 1p2w choke.

Inspection of Fig. 8's CM, DM and OC test circuits intuitively reveals the dc and low-frequency behaviors as well as the resonant characteristic behavior for each measurement, which facilitates model parameter extraction based on the measured impedance dataset. For example, the interwinding capacitance dominates the impedance of the OC test circuit at low frequency. Equations 5 through 7 describe the relevant impedances based on each of the three test setups.

$$Z_{CM}(j\omega) = R_0 + \sum_{i=1}^n \left(\frac{j\omega R_{Ci} L_{Ci}}{R_{Ci} - 2\omega^2 R_{Ci} L_{Ci} C_{Ci} + 2j\omega L_{Ci}} \right) \quad (5)$$

$$Z_{DM}(j\omega) = 2R_0 + \left[j\omega C_W + \left(\sum_{k=1}^m \frac{4j\omega R_{Dk} L_{Dk}}{R_{Dk} - 2\omega^2 R_{Dk} L_{Dk} C_{Dk} + 2j\omega L_{Dk}} + \frac{2R_0}{1 + 2j\omega R_0 C_W} \right)^{-1} \right]^{-1} \quad (6)$$

$$Z_{OC}(j\omega) = 2R_0 + \left[j\omega C_W + \left(\sum_{k=1}^m \frac{4j\omega R_{Dk} L_{Dk}}{R_{Dk} - 2\omega^2 R_{Dk} L_{Dk} C_{Dk} + 2j\omega L_{Dk}} + \frac{1}{j\omega C_W} \right)^{-1} \right]^{-1} \quad (7)$$

If each block has just one RLC circuit ($n = m = 1$), then equations 5 through 7 simplify as equations 8 through 10 for the CM, DM and OC test setups, respectively.

$$Z_{CM}(j\omega) = R_0 + \frac{j\omega L_C}{1 - 2\omega^2 L_C C_C + 2j\omega L_C / R_C} \quad (8)$$

$$Z_{DM}(j\omega) = 4R_0 + \frac{4j\omega L_D}{1 - 2\omega^2 L_D (C_D + 2C_W) + 2j\omega L_D / R_D} \quad (9)$$

$$Z_{OC}(j\omega) = 2R_0 + \frac{1}{j\omega(2C_W)} \frac{1 - 2\omega^2 L_D (C_D + 2C_W) + 2j\omega L_D / R_D}{1 - 2\omega^2 L_D (C_D + C_W) + 2j\omega L_D / R_D} \quad (10)$$

As shown in Fig. 4 and by the impedance expressions above, the typical behavior of the CM and DM impedances at lower frequencies is inductive, as expected, whereas there may be several resonant effects taking place at higher frequencies. In order to extract the component values of the behavioral model equivalent circuit, let's establish the following four premises, which when fulfilled enable a straightforward, equation-based parameter extraction.

1. At frequencies close to dc (f_0), the impedance of the choke is resistive and set by R_0 .
2. At a lower frequency f_1 , the inductive behavior dominates the impedance. Similarly, the interwinding capacitance sets the low-frequency impedance from the OC test.
3. A parallel resonant circuit with impedance Z_i causes a resonance at f_{ri} ; we can then neglect the influence of other resonant stages $Z_j, j \neq i$.
4. Resonant circuits Z_i and Z_{i+1} in series result in an anti-resonance at f_{ai} ; you can then neglect the influence of other resonant stages $Z_j, j \neq i, i+1$.

Thus, Table 1 extracts the model parameters for a 1p2w choke by suitably inspecting the behavior at dc, low frequency and the resonant frequencies. This procedure is equally applicable to characterizing both a CM choke (where the CM inductance is dominant) and a coupled inductor (where the DM inductance is higher than the CM inductance). If multiple resonances exist and capacitance C_W is nonzero, then an iterative extraction procedure is ideal.^[12]

Table 1. Expressions for model parameter extraction of a 1p2w ferrite choke.

Premise	Frequency	CM test	DM test
1	Close to dc	$R_0 \approx Z_{CM}(f_{C0})$	$R_0 \approx \text{Re}\{Z_{DM}(f_{D0})\}/4$
2	Low frequency	$L_C = \frac{ Z_{CM}(f_{C1}) }{2\pi f_{C1}}$	$L_D = \frac{ Z_{DM}(f_{D1}) }{8\pi f_{D1}}$
3	Main resonance	$C_C = \frac{1}{8\pi^2 f_{CR1}^2 L_C}$	$C_D = \frac{1}{8\pi^2 f_{DR1}^2 L_D} - 2C_W$
		$R_C = 2 Z_{CM}(f_{CR1}) $	$R_D = Z_{DM}(f_{DR1}) /2$
4	Higher-order resonances	$L_{Ci+1} = L_{Ci} \frac{1 - (f_{CAi}^2/f_{CRI+1}^2)}{(f_{CAi}^2/f_{CRI}^2) - 1}$	$L_{Di+1} = L_{Di} \frac{1 - (f_{DAi}^2/f_{DRI+1}^2)}{(f_{DAi}^2/f_{DRI}^2) - 1}$
		$C_{Ci+1} = C_{Ci} \frac{1 - (f_{CRI}^2/f_{CAi}^2)}{(f_{CRI+1}^2/f_{CAi}^2) - 1}$	$C_{Di+1} = C_{Di} \frac{1 - (f_{DRI}^2/f_{DAi}^2)}{(f_{DRI+1}^2/f_{DAi}^2) - 1}$
		$R_{Ci+1} = 2 Z_{CM}(f_{CRI+1}) $	$R_{Di+1} = Z_{DM}(f_{DRI+1}) /2$

Behavioral Model Structure For A Three-Phase Ferrite Choke

Extrapolating the same model structure and technique to a 3p3w choke, Fig. 9 shows the behavioral circuit model with equal and symmetrically spaced windings, conceiving a model structure similar to that for the 1p2w choke in Fig. 5.

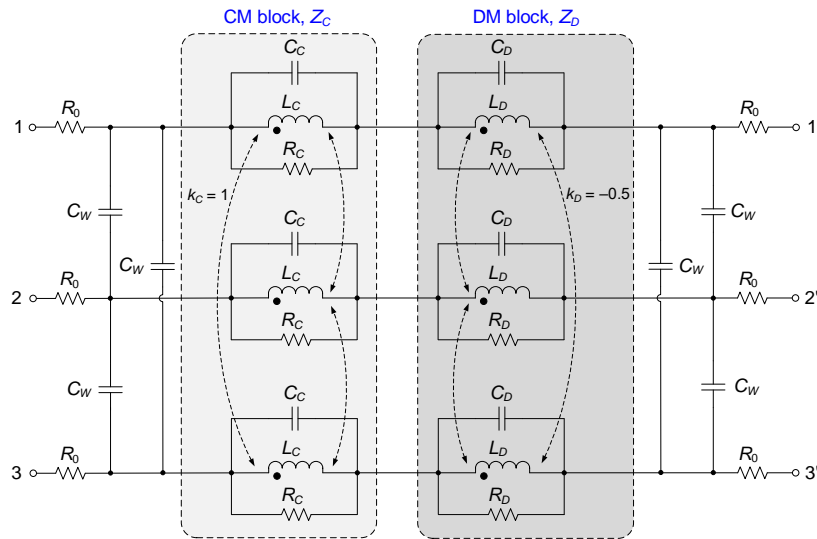


Fig. 9. Behavioral circuit model of a 3p3w ferrite choke with separate CM and DM blocks.

The CM triplets have coupling $k_C = 1$ to describe the CM behavior, whereas the DM triplets use $k_D = -0.5$ to avoid CM current exciting the DM block. Such coupling coefficients ensure that the CM and DM blocks are not cross-coupled and impart zero impedance for DM and CM currents, respectively. The remaining circuit parameters have the same meaning as in the case of the 1p2w choke.

Fig. 10 illustrates for the 3p3w case the CM and DM circuit reduction from coupled to uncoupled inductors and lastly to a parallel RLC circuit arrangement. As before, it is quite straightforward for three-phase realizations to transition between two-terminal and multiterminal equivalent circuits by scaling the component values as indicated.

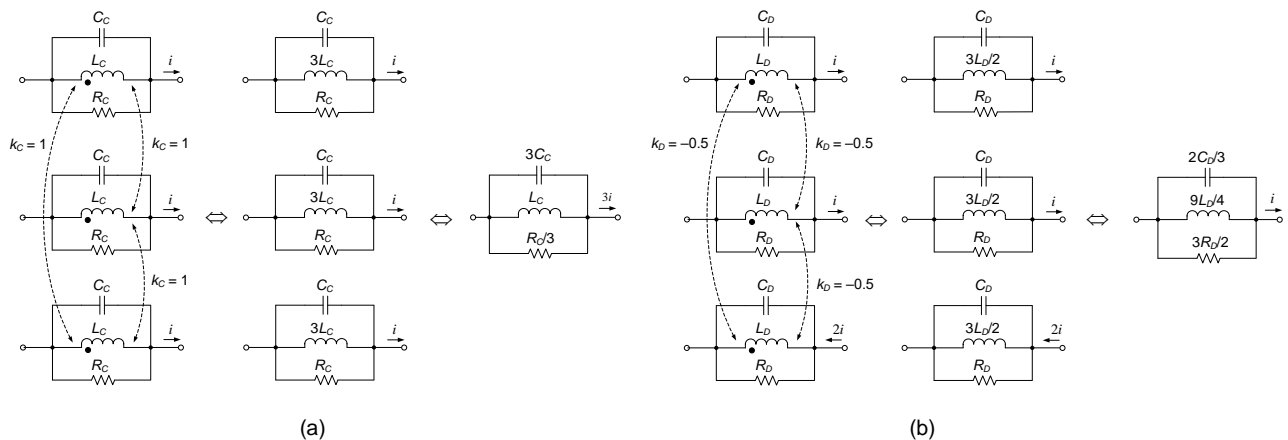


Fig. 10. Three-phase equivalent circuit of CM block with CM current (a) and DM block with DM current (b).

Fig. 11a presents the generalized circuit model for a three-winding magnetic—effectively an extension of the two-winding model in Fig. 7a. As before, each block contains one or multiple parallel RLC circuits connected in series to model the main and higher-order resonances, as shown in Fig. 11b.

Similarly conceived is a model for a 3p4w choke, which is left as an exercise for the interested reader. As such, the model structure is universal in nature because it caters to different types of magnetics, both single phase and three phase.

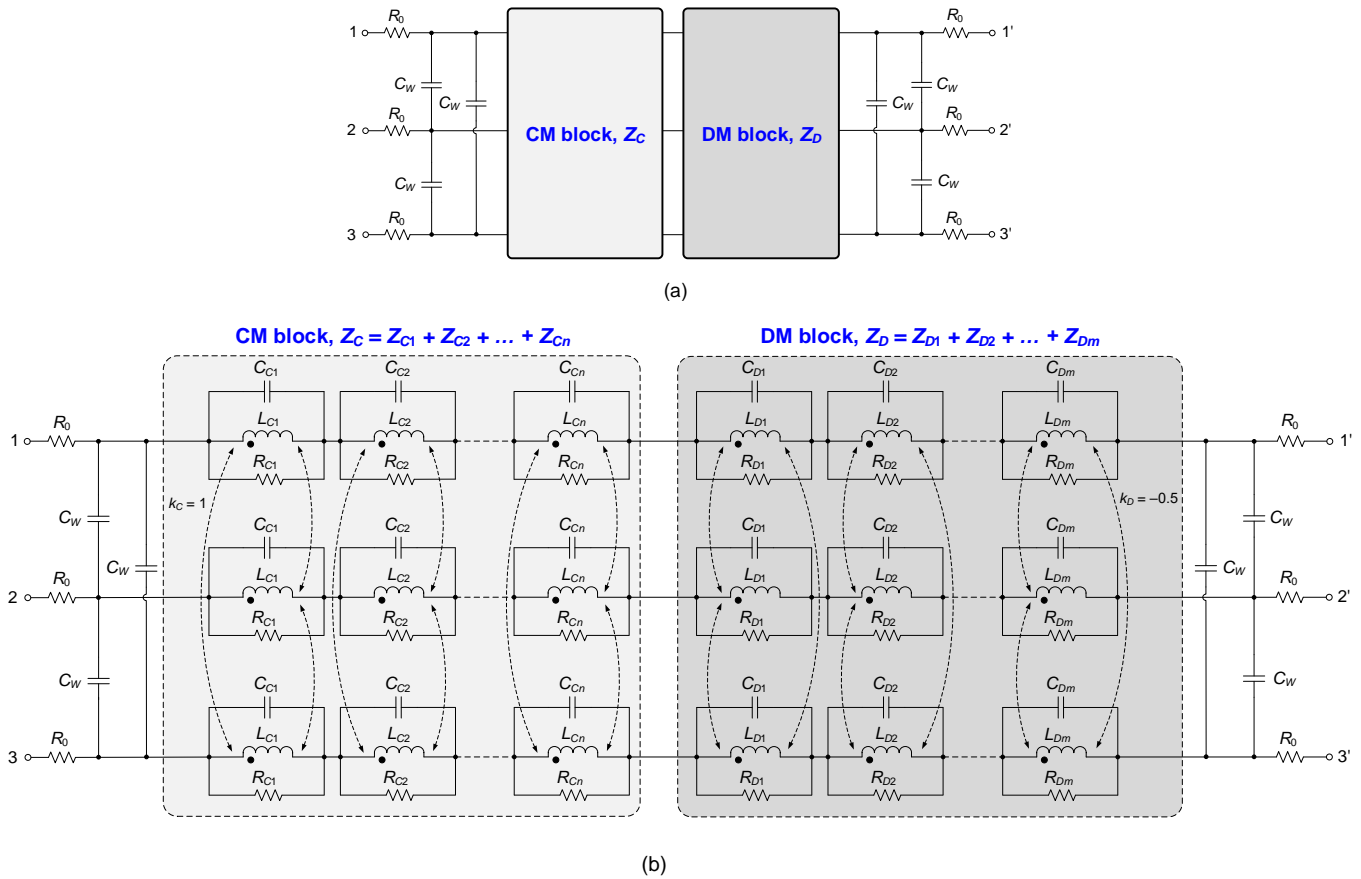
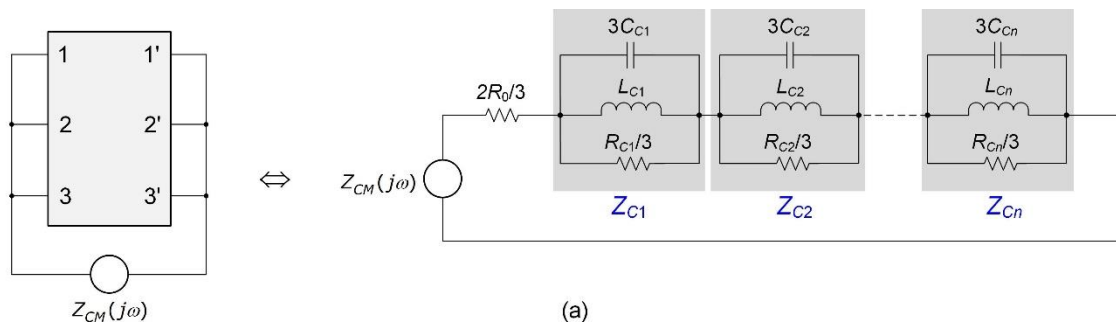


Fig. 11. Generalized 3p3w choke model consisting of CM and DM blocks (a) with additional RLC elements to model high-frequency resonant behaviors (b).

Parameter Extraction For A Three-Phase Ferrite Choke

Fig. 12 illustrates the measurement setups for CM, DM and OC impedance tests to characterize a 3p3w choke. Also shown is the corresponding equivalent circuit for each test based on suitable manipulation of the model in Fig. 11.



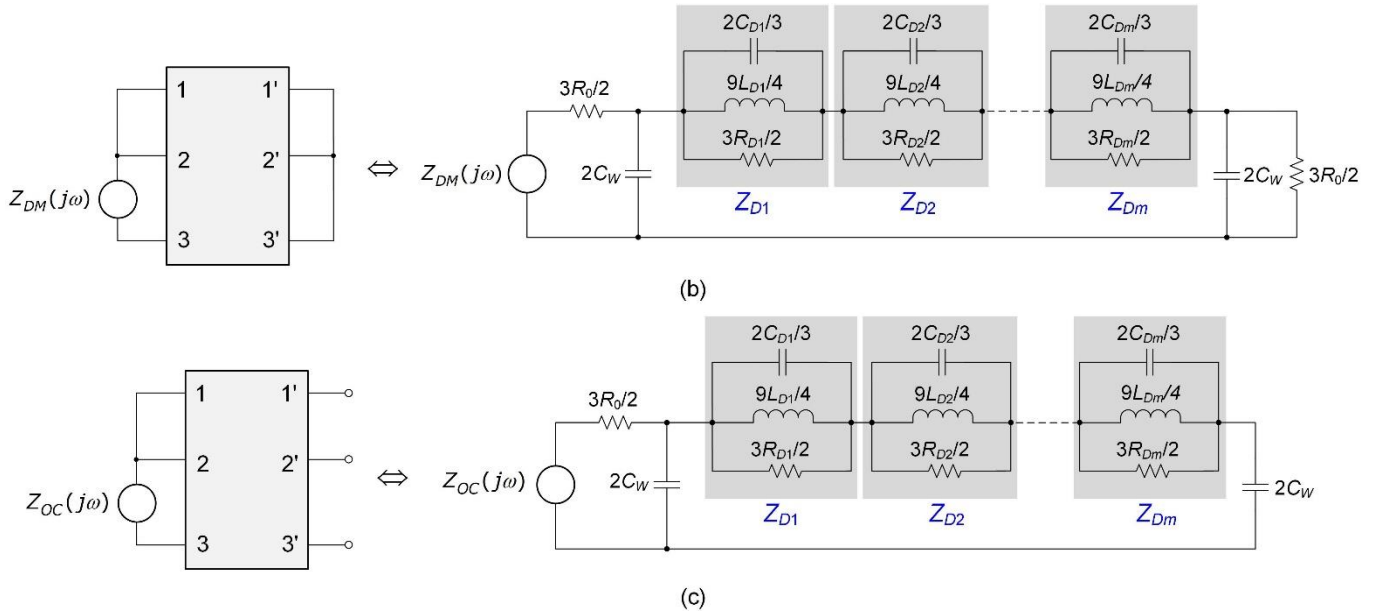


Fig. 12. Equivalent circuits corresponding to CM (a), DM (b), and OC (c) impedance measurement setups for parameter extraction of a 3p3w choke.

With impedance of each of the three test circuits described as follows, extraction of the model parameters is analogous to that outlined earlier for the 1p2w choke. If the CM and DM blocks each contain just one RLC circuit ($n = m = 1$), then equations 11 through 13 simplify as equations 14 through 16 for the CM, DM and OC test setups, respectively:

$$Z_{CM}(j\omega) = \frac{2R_0}{3} + \sum_{i=1}^n \left(\frac{j\omega R_{Ci} L_{Ci}}{R_{Ci} - 3\omega^2 R_{Ci} L_{Ci} C_{Ci} + 3j\omega L_{Ci}} \right) \quad (11)$$

$$Z_{DM}(j\omega) = 3R_0 + \left[2j\omega C_W + \left(\frac{3}{2} \sum_{k=1}^m \frac{3j\omega R_{Dk} L_{Dk}}{2R_{Dk} - 3\omega^2 R_{Dk} L_{Dk} C_{Dk} + 3j\omega L_{Dk}} + \frac{3R_0/2}{1 + 3j\omega R_0 C_W} \right)^{-1} \right]^{-1} \quad (12)$$

$$Z_{OC}(j\omega) = \frac{3R_0}{2} + \left[2j\omega C_W + \left(\frac{3}{2} \sum_{k=1}^m \frac{3j\omega R_{Dk} L_{Dk}}{2R_{Dk} - 3\omega^2 R_{Dk} L_{Dk} C_{Dk} + 3j\omega L_{Dk}} + \frac{1}{2j\omega C_W} \right)^{-1} \right]^{-1} \quad (13)$$

$$Z_{CM}(j\omega) = \frac{2R_0}{3} + \frac{j\omega L_C}{1 - 3\omega^2 L_C C_C + 3j\omega L_C / R_C} \quad (14)$$

$$Z_{DM}(j\omega) = 3R_0 + \frac{3j\omega L_D}{2 - 3\omega^2 L_D (C_D + 3C_W) + 3j\omega L_D / R_D} \quad (15)$$

$$Z_{OC}(j\omega) = \frac{3R_0}{2} + \frac{1}{j\omega (4C_W)} \frac{2 - 3\omega L_D (C_D + 3C_W) + 3j\omega L_D / R_D}{2 - 3\omega^2 L_D (C_D + 3C_W/2) + 3j\omega L_D / R_D} \quad (16)$$

Similar to the 1p2w choke, parameter extraction for a 3p3w choke is then deduced directly, as classified in Table 2 in terms of the final expressions.

Table 2. Expressions for model parameter extraction of a 3p3w ferrite choke.

Premise	Frequency	CM test	DM test	OC test
1	Close to dc	$R_0 \approx \frac{3}{2} Z_{CM}(f_{C0})$	$R_0 \approx \frac{1}{3} \text{Re}\{Z_{DM}(f_{D0})\}$	-
2	Low frequency	$L_C = \frac{ Z_{CM}(f_{C1}) }{2\pi f_{C1}}$	$L_D = \frac{2 Z_{DM}(f_{D1}) }{9\pi f_{D1}}$	$C_W = \frac{1}{8\pi f_{OC1} Z_{OC}(f_{OC1}) }$
3	Main resonance	$C_C = \frac{1}{12\pi^2 f_{CR1}^2 L_C}$	$C_D = \frac{1}{6\pi^2 f_{DR1}^2 L_D} - 3C_W$	-
		$R_C = 3 Z_{CM}(f_{CR1}) $	$R_D = \frac{2}{3} Z_{DM}(f_{DR1}) $	
4	Higher-order resonances	$L_{Ci+1} = L_{Ci} \frac{1 - (f_{CAi}^2 / f_{CRi+1}^2)}{(f_{CAi}^2 / f_{CRi}^2) - 1}$	$L_{Di+1} = L_{Di} \frac{1 - (f_{DAi}^2 / f_{DRi+1}^2)}{(f_{DAi}^2 / f_{DRi}^2) - 1}$	-
		$C_{Ci+1} = C_{Ci} \frac{1 - (f_{CRi}^2 / f_{CAi}^2)}{(f_{CRi+1}^2 / f_{CAi}^2) - 1}$	$C_{Di+1} = C_{Di} \frac{1 - (f_{DRi}^2 / f_{DAi}^2)}{(f_{DRi+1}^2 / f_{DAi}^2) - 1}$	
		$R_{Ci+1} = 3 Z_{CM}(f_{CRi+1}) $	$R_{Di+1} = \frac{2}{3} Z_{DM}(f_{DRi+1}) $	

Practical Example

Let's use a CM choke with ferrite core as a test case to prove the effectiveness of the proposed method both in terms of accuracy and ease of implementation. You can perform small-signal impedance measurements at low excitation levels with an impedance analyzer, a spectrum analyzer with a tracking generator or a vector network analyzer (VNA). In this case, I used an Omicron Labs Bode 100 VNA to measure the CM and DM impedances to a maximum frequency of 40 MHz using a single-port measurement technique.^[14]

Fig. 13 shows a practical implementation^[12] using a two-stage filter design with grid-side and regulator-side CM chokes of 2 mH and 4 mH, respectively.



Fig. 13. A totem-pole power factor correction ac-dc and half-bridge LLC dc-dc regulator include a single-phase EMI filter with ferrite choke.

The 4-mH choke (for which the CM and DM impedance characteristics are plotted in Fig. 4) is a custom ferrite design manufactured by Yaxin Electronics that provides high DM inductance in addition to the expected high CM impedance.

With Table 1 as a reference, Table 3 steers the calculation flow of model parameters for this example based on the selected test frequencies and respective impedance values taken from the measured impedance plots (with annotations) in Fig. 14, the same data provided in Fig. 4. Note that DM calculations are optional for a CM choke—they are included here because the DM impedance is higher than normal.

Table 3. Model parameter calculation flow based on the CM, DM and OC impedance measurements.

Test setup	Test frequency	Measured impedance	Calculated model parameter
CM	$f_{C1} = 10 \text{ kHz}$	$ Z_{CM}(f_{C1}) = 250 \Omega$	$L_{C1} = \frac{ Z_{CM}(f_{C1}) }{2\pi f_{C1}} = 4 \text{ mH}$
	$f_{CR1} = 230 \text{ kHz}$	$ Z_{CM}(f_{CR1}) = 13 \text{ k}\Omega$	$C_{C1} = \frac{1}{8\pi^2 f_{CR1}^2 L_{C1}} = 60 \text{ pF}$ $R_{C1} = 2 Z_{CM}(f_{CR1}) = 26 \text{ k}\Omega$
	$f_{CA1} = 24 \text{ MHz}$ $f_{CR2} = 32 \text{ MHz}$	$ Z_{CM}(f_{CR2}) = 220 \Omega$	$L_{C2} = L_{C1} \frac{1 - (f_{CA1}^2/f_{CR2}^2)}{(f_{CA1}^2/f_{CR1}^2) - 1} = 161 \text{ nH}$ $C_{C2} = C_{C1} \frac{1 - (f_{CR1}^2/f_{CA1}^2)}{(f_{CR2}^2/f_{CA1}^2) - 1} = 77 \text{ pF}$ $R_{C2} = 2 Z_{CM}(f_{CR2}) = 440 \Omega$
OC	$f_{OC1} = 10 \text{ kHz}$	$ Z_{OC}(f_{OC1}) = 8 \text{ M}\Omega$	$C_W = \frac{1}{4\pi f_{OC1} Z_{OC}(f_{OC1}) } = 1 \text{ pF}$
DM	$f_{D0} = 10 \text{ Hz}$	$ Z_{DM}(f_{D0}) = 80 \text{ m}\Omega$	$R_0 \approx \text{Re}\{Z_{DM}(f_{D0})\}/4 = 20 \text{ m}\Omega$
	$f_{D1} = 100 \text{ kHz}$	$ Z_{DM}(f_{D1}) = 49 \Omega$	$L_{D1} = \frac{ Z_{DM}(f_{D1}) }{8\pi f_{D1}} = 19.5 \mu\text{H}$
	$f_{DR1} = 2.2 \text{ MHz}$	$ Z_{DM}(f_{DR1}) = 24 \text{ k}\Omega$	$C_{D1} = \frac{1}{8\pi^2 f_{DR1}^2 L_{D1}} - 2C_W = 133 \text{ pF}$ $R_{D1} = Z_{DM}(f_{DR1}) /2 = 12 \text{ k}\Omega$
	$f_{DA1} = 29 \text{ MHz}$ $f_{DR2} = 33 \text{ MHz}$	$ Z_{DM}(f_{DR2}) = 106 \Omega$	$L_{D2} = L_{D1} \frac{1 - (f_{DA1}^2/f_{DR2}^2)}{(f_{DA1}^2/f_{DR1}^2) - 1} = 26 \text{ nH}$ $C_{D2} = C_{D1} \frac{1 - (f_{DR1}^2/f_{DA1}^2)}{(f_{DR2}^2/f_{DA1}^2) - 1} = 448 \text{ pF}$ $R_{D2} = Z_{DM}(f_{DR2}) /2 = 53 \Omega$

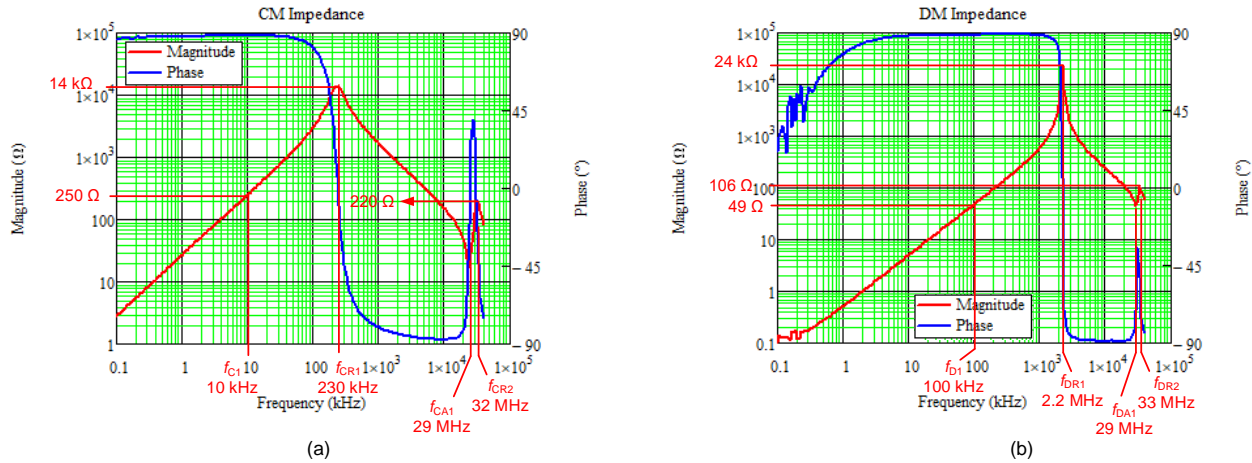


Fig. 14. Exemplary measured CM (a) and DM (b) impedance plots with identified frequencies and impedances for parameter extraction calculations.

Subsequently, Fig. 15a shows the derived SIMPLIS behavioral model based on the calculations from Table 3. Note the highlighted connection in blue that effectively reverses the winding dot polarity to establish $k_D = -1$ in the DM block.

Fig. 15 parts b and c show the simulated CM and DM impedance results, providing a close match to the magnitude and phase data of Fig. 14 as expected. The dashed lines in these plots represent the response without the second stage in the CM and DM blocks that model the higher-order resonant behavior.

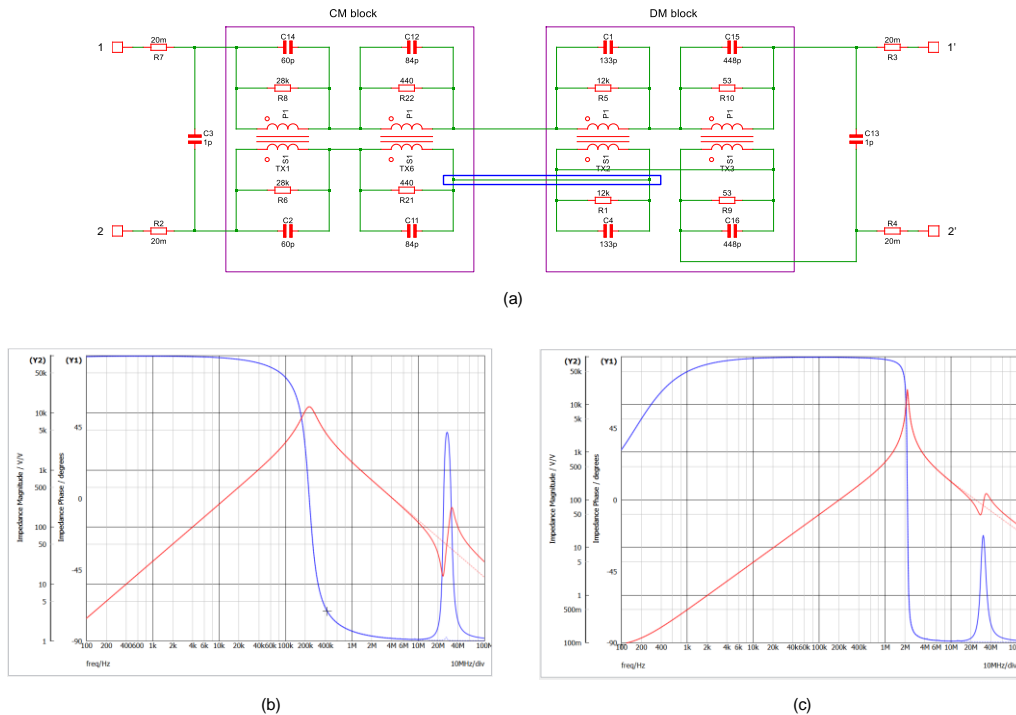


Fig. 15. Derived SIMPLIS behavioral model (a); simulation model results for CM impedance (b); and DM impedance (c) that closely match the measured data in Fig. 14.

Summary

Having accurate, easy-to-use, computationally efficient choke models for system-level simulations in both the time and frequency domains has become an important litmus test in the design of EMI filter circuits. In response to that need, this article details the derivation of a behavioral model for the CM and DM impedance behaviors of a ferrite-cored choke. Using a CM choke with ferrite core as a test case proves the effectiveness of the proposed method in terms of accuracy and ease of implementation.

The measured CM and DM impedance curves are synthesized into a behavioral model suitable for implementation in any circuit simulator to facilitate the design of EMI filters. The model structure is universal in that it accommodates DM and CM chokes, both single phase and three phase, and operates in both the time and frequency domains.

References

1. ["How Active EMI Filter ICs Reduce Common-Mode Emissions In Single- And Three-Phase Applications \(Part 1\): An Overview"](#) How2Power Today, November 2023 Issue.
2. [TPSF12C1 product page.](#)
3. [TPSF12C3 product page.](#)
4. ["TPSF12C1 and TPSF12C3 power-supply filter IC FAQs"](#) by Timothy Hegarty, TI E2E design support forums, August 2023.
5. ["On Modeling the Common Mode Inductor"](#) by Mark Nave, proceedings of the IEEE International Symposium on Electromagnetic Compatibility, July 12-Aug. 16, 1991, pp. 452-457.
6. ["Common-Mode Choke Coils Characterization"](#) by Konstantin Kostov and Jorma Kyyra, proceedings of the 2009 13th European Conference on Power Electronics and Applications, Sept. 8-10, 2009, pp. 1-9.
7. ["Design and Characterization of Single-Phase Power Filters"](#) by Konstantin Kostov, Ph.D. dissertation, Helsinki University of Technology, 2009.
8. ["The Three-Phase Common-Mode Inductor: Modeling and Design Issues"](#) by Marcelo Lobo Heldwein, Luca Dalessandro, and Johann W. Kolar, IEEE Transactions in Industrial Electronics 58, no. 8 (August 2011): pp. 3254-3274.
9. ["Modeling the Magnetic Behavior of N-Winding Components: Approaches for Unshackling Switching Superheroes"](#) by Alex Hanson and David Perreault, IEEE Power Electronics Magazine 7, no. 1 (March 2020), pp. 35-45.
10. [Ferrite Materials](#), TDK web page, accessed Jan. 11, 2024.
11. [Welcome to the "Magnetic Design Tool,"](#) TDK web page, accessed Jan. 11, 2024.
12. [1-kW, 80+ Titanium, GaN CCM Totem Pole Bridgeless PFC and Half-Bridge LLC With LFU Reference Design](#), Texas Instruments reference design No. TIDA-010062, September 2019.
13. ["Behavioral Modeling of Chokes for EMI Simulations in Power Electronics"](#) by Ivica Stevanovic, Stanislav Skibin, Mika Masti, and Matti Laitinen, IEEE Transactions on Power Electronics 28, no. 2 (February 2013), pp. 695-705.
14. ["Impedance Measurements Using the Bode 100"](#) by Tobias Schuster and Florian Hämmerle, Omicron Lab application note, 2020.

About The Author



Timothy Hegarty is a senior member of technical staff (SMTS) in the Switching Regulators business unit at Texas Instruments. With over 25 years of power management engineering experience, he has written numerous conference papers, articles, seminars, white papers, application notes and blogs. Tim's current focus is on enabling technologies for high-frequency, low-EMI, isolated and nonisolated regulators with wide input voltage range, targeting industrial, communications and automotive applications in particular. He is a senior member of the IEEE and a member of the IEEE Power Electronics, Industrial Applications and EMC Societies.

For more on EMI and EMC topics in power supply design, see the How2Power's [Power Supply EMI Anthology](#).